mathematics

MDPI

Article

A Particle Swarm Optimization-Based Ensemble Broad Learning System for Intelligent Fault Diagnosis in Safety-Critical Energy Systems with High-Dimensional Small Samples

Jiasheng Yan [1,2], Yang Sui [1,2,*] and Tao Dai [1,2]

[1] School of Nuclear Science and Technology, University of South China, Hengyang 421001, China; yanjiasheng@stu.usc.edu.cn (J.Y.); daitao@stu.usc.edu.cn (T.D.)
[2] Key Laboratory of Advanced Nuclear Energy Design and Safety, Ministry of Education, University of South China, Hengyang 421001, China
* Correspondence: suiyang@usc.edu.cn

Abstract: Intelligent fault diagnosis (IFD) plays a crucial role in reducing maintenance costs and enhancing the reliability of safety-critical energy systems (SCESs). In recent years, deep learning-based IFD methods have achieved high fault diagnosis accuracy extracting implicit higher-order correlations between features. However, the excessive long training time of deep learning models conflicts with the requirements of real-time analysis for IFD, hindering their further application in practical industrial environments. To address the aforementioned challenge, this paper proposes an innovative IFD method for SCES that combines the particle swarm optimization (PSO) algorithm and the ensemble broad learning system (EBLS). Specifically, the broad learning system (BLS), known for its low time complexity and high classification accuracy, is adopted as an alternative to deep learning for fault diagnosis in SCES. Furthermore, EBLS is designed to enhance model stability and classification accuracy with high-dimensional small samples by incorporating the random forest (RF) algorithm and an ensemble strategy into the traditional BLS framework. In order to reduce the computational cost of the EBLS, which is constrained by the selection of its hyperparameters, the PSO algorithm is employed to optimize the hyperparameters of the EBLS. Finally, the model is validated through simulated data from a complex nuclear power plant (NPP). Numerical experiments reveal that the proposed method significantly improved the diagnostic efficiency while maintaining high accuracy. In summary, the proposed approach shows great promise for boosting the capabilities of the IFD models for SCES.

Keywords: safety-critical energy systems; intelligent fault diagnosis; ensemble broad learning system; random forest; particle swarm optimization

MSC: 68T05

Academic Editor: Phuc Do

Received: 24 December 2024
Revised: 7 February 2025
Accepted: 11 February 2025
Published: 27 February 2025

Citation: Yan, J.; Sui, Y.; Dai, T. A Particle Swarm Optimization-Based Ensemble Broad Learning System for Intelligent Fault Diagnosis in Safety-Critical Energy Systems with High-Dimensional Small Samples. *Mathematics* **2025**, *13*, 797. https://doi.org/10.3390/math13050797

1. Introduction

1.1. Problem Statement

Safety-critical energy systems (SCESs) refer to complex, large-scale energy systems where system failures or malfunctions can potentially lead to severe consequences, such as loss of life, serious injuries, equipment damage, or environmental harm. The nuclear energy system serves as a typical example of a SCES, as a catastrophic nuclear disaster would have devastating impacts on all aspects of human society [1,2]. As energy systems continue to

expand in scale and complexity, higher demands are placed on their security and reliability, necessitating the early detection and identification of potential abnormalities and faults, as well as the implementation of real-time fault-tolerant operations to minimize performance degradation and avoid dangerous situations [3,4]. Fault diagnosis, the process of identifying or predicting system faults to assess their type, location, and severity, provides powerful guarantees for the safety and reliability of modern complex, large-scale process systems, such as SCESs, by delivering accurate and timely fault information [5,6]. Traditionally, fault diagnosis is heavily dependent on the abundant experience and huge expert knowledge of engineers. However, in engineering scenarios, system users would like an automatic method to shorten the maintenance cycle and improve the diagnosis accuracy [7]. Intelligent fault diagnosis utilizes artificial intelligence technologies in the process of fault diagnosis to automatically extract features and identify faults, making the process intelligent and automated while simultaneously reducing the cost of manual feature analysis and avoiding excessive reliance on prior knowledge [8,9]. Therefore, the development of an efficient and accurate IFD method specifically tailored for SCES is of paramount importance.

During the last few decades, extensive efforts have been dedicated to IFD, resulting in the development of a wide array of diagnostic models [10]. Generally, IFD models can be categorized into model-based and data-driven models [11,12]. Regarding the model-based methods, accurate quantitative mathematical models need to be established based on strong assumptions and physical knowledge, and the fault diagnosis is usually accomplished through residual generation or evaluation concepts [13,14]. Conversely, whereas for changeable operational conditions and complicated working environment in SCESs, there are difficulties in accurate fault modeling [15]. Furthermore, model-based methods, though ideal for systems with limited inputs, outputs, or state variables, become prohibitively costly and inefficient for complex, large-scale systems with large amounts of data [16]. It is evident that model-based fault diagnosis methods are not well suited for the IFD of SCESs. In contrast, data-driven fault diagnosis methods, which are model-independent methods, can adaptively extracting decision rules from data with no reliance on precise analytical models and domain knowledge [17–20]. It is clear that the data-driven methods are better suited for the IFD of SCESs.

Along with the development and integration of big data and artificial intelligence technology, data-driven methods based on machine learning have been applied widely in the field of fault diagnosis. Researchers have proposed various methods for IFD, including neural networks [21], random forest classifiers [22], k-means clustering [23], support vector machines [24], gaussian process regression [25], logistic regression [26], and many more. Deep learning, a subset of neural networks, is generally composed of multiple layers to learn data features with multiple levels of abstraction by mining complex knowledge from simpler concepts [27]. Due to their powerful feature learning and data analysis capabilities, deep learning methods significantly improve fault diagnosis accuracy. Du et al. [28] proposed a knowledge-embedded deep belief network method, which was experimentally validated to achieve satisfactory performance in diagnosing electronic–thermal and thermal–thermal multiple faults of chillers, even when training data for certain faults was absent. Seghiour et al. [29] proposed a deep learning method based on an autoencoder neural network, validated with monitored data from a real photovoltaic system in Algeria, demonstrating its effectiveness in detecting and classifying various photovoltaic system fault types. Harrou et al. [30] proposed a semi-supervised deep learning method for fault detection in photovoltaic systems, demonstrating exceptional performance in accurately identifying faults such as partial shading, inverter failures, and others. However, these deep structures suffer from a mass of iterative training processes that consume time and computational resources due to their large number of parameters and complicated hand-

designed structures. What is more, it is not easy to rapidly update its deep architecture parameters, because it involves the entire network when facing newly added samples [31].

The broad learning system (BLS) is the new model proposed by C. L. Philip Chen, which can replace deep learning for data training [32]. Compared to deep learning, BLS is a low-cost, high-performance method that overcomes the drawbacks of time consumption, excessive hyperparameters, and complex structures [33]. The BLS can adaptively expand the width of a model by adjusting its feature set, neural nodes, and input samples, effectively avoiding the time-consuming challenges associated with deep stacking structures [34]. Moreover, BLS tends to process data more efficiently and achieve better diagnostic results in small-sample fault diagnosis tasks. Deep learning typically requires large amounts of data to extract meaningful features, and small samples can lead to overfitting, poor generalization, and less reliable results in fault diagnosis. In contrast, BLS, which focuses on learning from a broader set of features rather than relying on deep hierarchical representations, is more suited to small-sample fault diagnosis due to its ability to generalize better with small samples. However, the above-mentioned BLS-based method investigation is partial to low-dimensional data scenarios.

High-dimensional data often refer to datasets with hundreds or even thousands of features [35,36]. Given the complex inherent system composition of the SCES, coupled with numerous and various of equipment, SCESs generate a multitude of monitoring variables, leading to high-dimensional characteristics in the operational data [37]. In high-dimensional classification, if features substantially outnumber instances, classifiers might not generalize well using the characteristics of the training data [36]. Therefore, in the field of intelligent fault diagnosis for safety-critical energy systems, high-dimensional data has emerged as a critical challenge that must be addressed for effective model training. Recently, multi-learner ensemble learning methods have been considered as a promising strategy to deal with high-dimensional data modeling. Li et al. [38] proposed the semi-supervised classification model with optimized graph construction and its enhanced framework for hybrid subspace ensemble based on optimized graph construction, which integrates multiple hybrid subspace models by combining predefined graphs, adaptive graphs, and regularization methods to effectively improve the classification performance of high-dimensional data, and the experimental results showed excellent results. Zhao and Ye [39] proposed the high-dimensional ensemble learning classification algorithm, which effectively improves the classification performance of high-dimensional data through feature space reconstruction and classifier integration and experimentally verifies its research and application value. Inspired by the idea of integration, scholars have continuously attempted to integrate BLS with multi-learner ensemble learning. Zhao et al. [40] proposed a novel transformer fault diagnosis model that utilizes a Filter–Wrapper Combined Feature Selection method and an AdaBoost-integrated weighted broad learning system. Cheng et al. [41] proposed a data-driven fault detection and diagnosis method via the intensive integration of principal component analysis and a BLS, where fast and accurate fault detection and diagnosis implementation could be easily accomplished. However, the above research works mainly focused on high-dimensional large-sample scenarios.

1.2. Research Motivation

Inspired by the problem statement, we focused on the strong research motivation to develop a novel IFD model based on BLS and ensemble learning for high-dimensional, small-sample fault diagnosis of SCESs. Driven by this motivation, our research aims to (1) provide a definition of EBLS in the proposed model; (2) propose an algorithm to detail the fault diagnosis process; (3) apply the proposed model to representative cases to validate its effectiveness.

1.3. Research Gap

Although IFD has been widely applied in the industrial sector, methods specifically designed for IFD in SCESs are still scarce. Most existing fault diagnosis research focuses on general industrial applications or relatively simpler systems, often overlooking the unique challenges posed by SCESs. For instance, SCESs typically involve highly complex structures, massive real-time data streams, and high-dimensional, small-sample data, making it difficult for traditional fault diagnosis methods to meet the high safety, real-time, and reliability requirements. In the existing research, Yao et al. proposed a novel IFD method for SCESs that integrates uncertainty-aware Bayesian deep learning [2]. Süle et al. proposed a P-graph-based multi-objective risk analysis and redundancy allocation method for SCESs [1]. However, these methods have limitations when applied to high-dimensional small samples.

Additionally, to build an efficient and accurate EBLS model, it is often necessary to fine-tune multiple hyperparameters to achieve optimal performance [42]. Traditionally, hyperparameter tuning has relied on the researcher's experience and prior knowledge, with adjustments made manually over time. However, this process is not only time-consuming and labor-intensive but also prone to human bias, making it difficult to reach the global optimum, especially when dealing with complex or large-scale problems [43]. As a result, optimizing algorithms to automate the hyperparameter tuning of TBLS models has become increasingly important. Recent advancements in heuristic algorithms have further demonstrated their versatility and efficiency in solving optimization problems across diverse domains. For instance, ant colony optimization (ACO) has been effectively employed in 3D path planning on remote sensing images to achieve energy-efficient solutions [44]. Similarly, rat swarm optimization (RSO) has shown promising results in addressing combinatorial optimization problems, such as the quadratic assignment problem [45]. Additionally, hybrid approaches like the genetic and penguin search optimization algorithm (GA-PSEOA) have been utilized for efficient flow shop scheduling, showcasing their potential in multi-objective optimization tasks [46]. In the context of hyperparameter optimization, ACO is prone to local optima in high-dimensional spaces, GA's reliance on crossover and mutation leads to slow convergence, and SA, though capable of finding the global optimum, suffers from slow convergence and prolonged escape times from local optima. In contrast, particle swarm optimization (PSO) stands out for its simplicity, efficiency, and adaptability, making it particularly suitable for high-dimensional, small-sample problems. By simulating the collective movement of particles in the search space, PSO efficiently identifies the optimal hyperparameter configuration, overcoming the limitations of manual tuning. Its reduced computational demands for global optimization, strong adaptability, and rapid convergence make it ideal for high-dimensional, nonlinear problems, positioning PSO as a reliable and effective solution for hyperparameter tuning in EBLS models.

1.4. Contribution Statement

Motivated by the above analysis and review, a PSO-based EBLS, including the ensemble broad learning system (EBLS) and the particle swarm optimization (PSO) algorithm, is proposed in this article. The major contributions contain the following parts:

(1) This paper introduces a novel IFD approach for SCESs, where the BLS method is employed as an alternative to deep learning techniques for fault diagnosis.
(2) We propose an EBLS framework that integrates the random forest(RF)algorithm and an ensemble strategy into the traditional BLS model, designed to handle high-dimensional small samples for improved stability and classification accuracy.
(3) The PSO algorithm is utilized to optimize the hyperparameters of the EBLS framework, leading to reduced computational costs and improved performance.

The rest of this paper is organized as follows: In Section 2, the BLS, RF, and PSO algorithms are introduced. In Section 3, the definitions of the EBLS methods and PSO-EBLS methods are provided. In Section 4, a detailed analysis, along with graphical and tabular results, is presented in Section 4. Finally, the paper is concluded in Section 5.

2. Preliminaries

In this section, we will delve into the architecture of the BLS and the RF, along with their respective mathematical formulations. After that, a brief introduction of PSO algorithm is given.

2.1. BLS

BLS is an improved flat network comprising three primary components: (1) feature mapping, (2) enhancement, and (3) dynamic weight update. A typical representation of BLS is shown in Figure 1, while Figure 2 presents the computational flowchart of BLS, with its mathematical formulations briefly outlined as follows.

In the feature mapping part, given a training dataset $\left\{(X,Y)\middle|X \in R^{N\times M}, Y \in R^{N\times 1}\right\}$ and n feature mappings ϕ, the feature mapping is as follows:

$$Z_i = \phi(XW_{ei} + \beta_{ei}),\ \ i = 1,\ 2, \ldots, n \tag{1}$$

where N is the number of samples, M denotes the dimension of samples, and Y represents the target of the fitting, which is a $N \times 1$ dimensional matrix, given that the multi-input single output modeling problem is the focus of this study. The weight W_{ei} and the bias term β_{ei} are randomly determined to develop the $i-$th mapping matrix Z_i. Therefore, the output of the n mapping nodes can be represented as

$$Z^n = [Z_1, Z_2, \ldots, Z_n] \tag{2}$$

where Z^n represents the entire output of the feature layer.

In the enhancement part, Z^n is utilized as the input of the nonlinear function ξ of the enhancement node. Then, the $j-$th enhancement node is as follows:

$$H_j = \xi\left(Z^n W_{hj} + \beta_{hj}\right),\ \ j = 1,\ 2, \ldots, n \tag{3}$$

where H_j is the output of the $j-$th enhancement node. Hence, the output of m mapping nodes can be denoted as

$$H^m \triangleq [H_1, H_2, \ldots, H_n] \tag{4}$$

The prediction output, without considering the dynamic weight update of incremental learning, is as follows:

$$\hat{Y} = A^m_n W^m_n = [Z^n\ ,\ H^m] W^m_n \tag{5}$$

where W^m_n is the weight matrix of the mapping layer and the enhancement layer to the output layer. It can be calculated using pseudoinverse, as follows:

$$\begin{aligned} W^m_n &= [A^m_n]^+ Y \\ &= \left[[A^m_n]^T A^m_n + \lambda I\right]^{-1} [A^m_n]^T Y \end{aligned} \tag{6}$$

where λ is a positive constant, and I is an identity matrix.

BLS provides three incremental learning strategies, namely adding enhancement nodes, feature mapping nodes, and inputting new data. The first method is considered an example of interpretation.

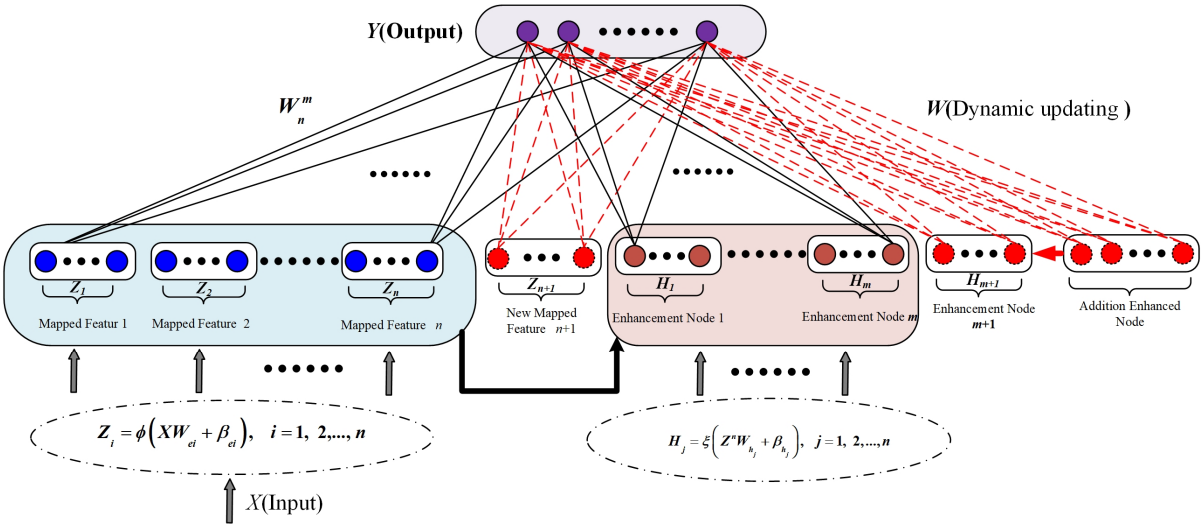

Figure 1. Architecture of BLS.

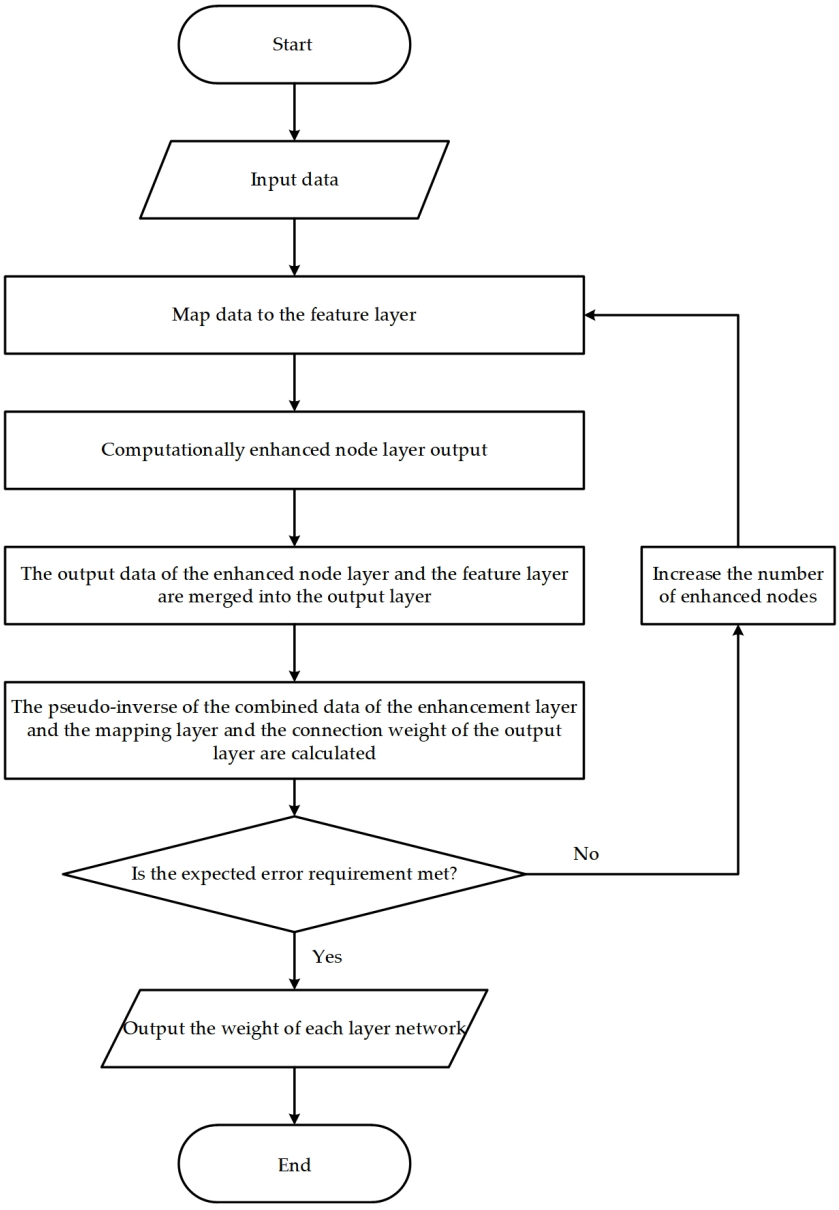

Figure 2. Computational flowchart of BLS.

Suppose that p enhancement nodes are added, the new matrix A_n^{m+1} is obtained as follows:

$$\begin{aligned} A_n^{m+1} &= [A_n^m\ ,\ H_{m+1}] \\ &= \left[A_n^m\ , \xi_{m+1}\left(Z^n W_{h(m+1)} + \beta_{h(m+1)}\right)\right] \end{aligned} \tag{7}$$

Therefore, the pseudoinverse of matrix A_n^{m+1} can be deduced as follows:

$$\left[A_n^{m+1}\right]^+ = \begin{bmatrix} [A_n^m]^+ - DB^T \\ B^T \end{bmatrix} \tag{8}$$

where

$$\begin{cases} D = [A_n^m]^+ H_{m+1} \\ B^T = \begin{cases} [C]^+ & if\ C = 0 \\ \left[1 + D^T D\right]^{-1} D^T [A_n^m]^+ & if\ C \neq 0 \end{cases}, \\ C = H_{m+1} - A_n^m D \end{cases} \tag{9}$$

Ultimately, the weight matrix W_n^{m+1} is updated as follows:

$$W_n^{m+1} = \begin{bmatrix} W_n^m - DB^T Y \\ B^T Y \end{bmatrix} \tag{10}$$

Equation (10) indicates that only the weights of the $(m+1)-$th group of enhancement nodes should be computed, thereby supporting the fast-learning characteristics of BLS.

2.2. RF

The RF algorithm operates by constructing a large ensemble of decision trees through the random sampling of observations and feature variables from the dataset. Each sampled subset generates a decision tree that establishes rules and prediction values based on its specific attributes. The final regression result is obtained by aggregating the rules and prediction values from all the trees in the forest. This approach makes random forest highly flexible, robust to noise, and less sensitive to data standardization.

2.3. PSO

The search process of the classical PSO algorithm is inspired by the behavior of birds in searching for food. In this algorithm, each particle represents a candidate solution of the optimization problem and searches the solution space at a certain speed. During the search process, each particle considers its current position, individual best position $pbset_i^t$, and the global best position of the entire population $gbset^t$ to adjust its speed and move towards the direction of the global optimal solution. The velocity and position of the particle p_i are represented as $x_i^t = \left[x_{i1}^t, x_{i2}^t, \ldots, x_{iD}^t\right]$ and $v_i^t = \left[v_{i1}^t, v_{i2}^t, \ldots, v_{iD}^t\right]$, respectively, where D is the size of the problem. Specifically, each particle updates its velocity and position based on its historical best position and the global best position, gradually approaching the global optimal solution:

$$v_i^{t+1} = \omega \cdot v_i^t + c_1 \cdot r_1 \cdot \left(pbset_i^t - x_i^t\right) + c_2 \cdot r_2 \cdot \left(gbset^t - x_i^t\right) \tag{11}$$

$$x_i^{t+1} = x_i^t + v_i^{t+1} \tag{12}$$

where ω represents the inertia weight, and the self-awareness and social awareness are regulated by the learning factors c_1 and c_2. These three parameters are responsible for adjusting and coordinating the ability of the algorithm to perform local and global optimization. In addition, two randomly generated numbers, r_1 and r_2, fall within the range of (0,1).

3. Materials and Methods

In this section, classical RF, PSO, and ensemble learning methods are used to enhance the performance of BLS for high-dimensional, small-sample IFD in SCESs. Initially, a novel model called the ensemble broad learning system (EBLS) is proposed by combining BLS with RF, and its structure is introduced. Then, PSO is applied to fine tune the hyperparameters, resulting in the construction of the PSO-EBLS model.

3.1. Definitions of EBLS Methods

The EBLS maintains the original structure of the BLS but improves its performance for high-dimensional, small-sample fault diagnosis (IFD) in SCESs by integrating random forest (RF) and ensemble learning techniques. We apply a RF-based feature selection strategy to identify key features that enhance the IFD performance. Next, we randomly sample data from these selected features to create multiple sub-training datasets using ensemble learning. Independent BLS models are then constructed based on these sub-training datasets, and their results are combined to provide a final diagnosis. The structure of the EBLS is shown in Figure 3, and a detailed description of the EBLS is provided below.

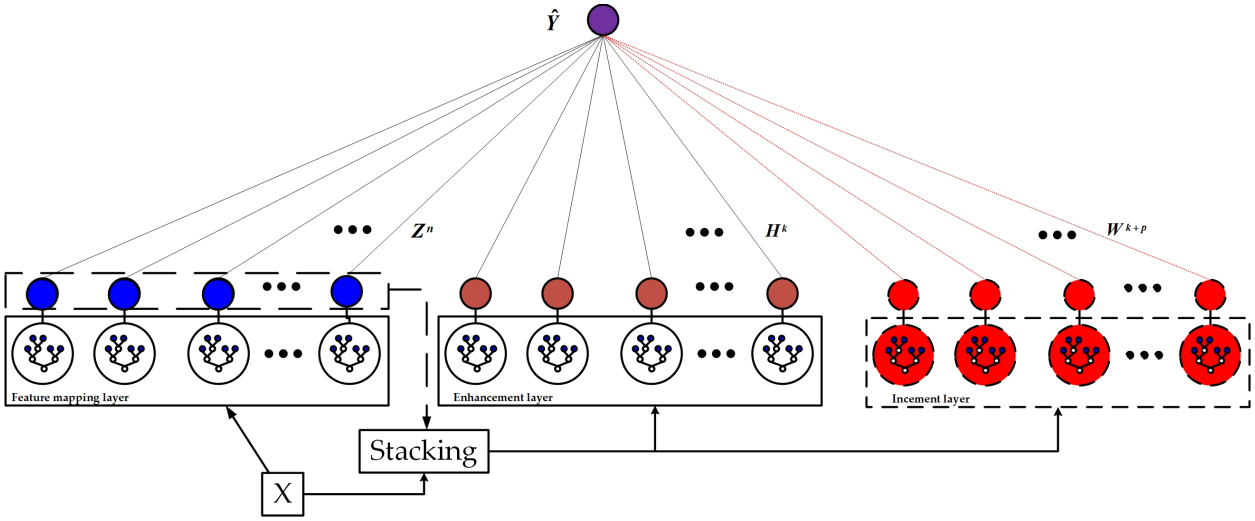

Figure 3. Architecture of the EBLS.

Assume that $X \in R^{n \times d}$ represents the input data, where n is the number of samples and d is the number of features, and $Y \in R^n$ represents the corresponding target labels. x_i is a row in X, and the data are often scaled to consistency, resulting in the scaled data matrix X_a, as shown in the Equation (13).

$$X_a = \text{StandardScaler}(X) \tag{13}$$

In order to enhance feature representation, a RF model consisting of T decision trees, is trained on the scaled data. The RF model can be described as a collection of trees, where each tree $t_K(X)$ generates a prediction based on the input data, as shown in Equation (14).

$$M(X) = \{t_1(x), t_2(x), \ldots t_T(x)\} \tag{14}$$

where $M(X)$ is a collection of trees.

Instead of using the final predictions, the RF maps x_i to the leaf nodes of each tree, producing a vector of leaf indices $S_i = [S_{i1}, S_{i2} \ldots, S_{iT}]$, which represent the new features for each sample. By aggregating these vectors, we create a feature matrix X_b, where each column corresponds to the leaf index output of a tree, as shown in Equation (15).

$$X_b = M(X) \tag{15}$$

This X_b can be combined with X_a to form an enhanced feature set $X_c \in R^{n\times(d+T)}$ in Equation (16).

$$X_c = [X_a, X_b] \tag{16}$$

Within the BLS, X_c is transformed by using linear or nonlinear mappings to produce the mapped features Z. The weights associated with the mapped nodes are represented by $W_Z \in R^{m\times(d+T)}$, where m is the number of mapped nodes, as shown in Equation (17).

$$Z = X_c \cdot W_Z \tag{17}$$

The enhancement layer inputs are generated to enrich the feature space and capture complex patterns. Enhancement nodes further transform the mapped features, resulting in enhancement features H, as shown in Equation (18).

$$H = Z \cdot W_E \tag{18}$$

where $W_E \in R^{m\times e}$ are the weights for the enhancement nodes, and e is the number of enhancement nodes.

The final feature matrix input into the BLS is obtained by concatenating the mapped features and the enhancement features, as shown in Equation (19).

$$H_f = [Z, H] \tag{19}$$

where H_f represents the final feature matrix that is input into the BLS.

Then, the candidate output $\widetilde{Y}$ is given by Equation (20).

$$\widetilde{Y} = H_f \cdot W_f + b_f \tag{20}$$

where W_f represents the weights; b_f is the bias term.

Finally, the true output Y is optimized by minimizing the regularized loss function, as given by Equation (21).

$$\min_{W_f} \left\| \widetilde{Y} - Y \right\|_2^2 + \alpha \left\| W_f \right\|_2^2 \tag{21}$$

where α is the regularization parameter.

The establishment of an EBLS includes the following parts [47]:

(1) **Feature selection:** Multiple factors are associated with fault occurrence in SCESs; however, certain faults may have less relevance, which can reduce the model's learning capability. Given that many features are independent of one another, we apply a RF feature selection strategy to automatically identify and filter the most relevant features.

(2) **Establish sub-training datasets:** The entire dataset is split into two subsets: a training dataset (of size N_1) and a test dataset (of size N_2). $\lfloor N_1 \cdot p \rfloor$ samples are chosen from the training dataset using the Bootstrapping technique where $0 < p < 1$ is the sampling ratio, and $\lfloor x \rfloor$ represents the largest integer no more than x. This sampling process is repeated T times to prepare T different sub-training datasets for training the sub-models.

(3) **Build the EBLS models:** In this model, each EBLS model is regarded as a weak learner in the ensemble learning model. Then, we combine multiple weak learners to form strong learners. Finally, the output of the EBLS model can be computed by

$$y_p = \frac{y_{p_1} + y_{p_2} + \cdots + y_{p_T}}{T} \tag{22}$$

where y_{p_i} is the predicted value of the $i-$th learner, while y_p is final predicted value.

3.2. Definitions of the PSO-EBLS Methods

There are three core parameters for the EBLS: number of feature node windows, number of nodes in each feature node window, and number of enhancement nodes. The EBLS model uses the pseudoinverse to compute the output weights instead of backpropagation, making the initial parameters crucial for the network's performance. High-quality initial parameters ensure a stable and accurate diagnosis. We use the PSO algorithm to optimize the EBLS and find the best initial parameters, then apply the model for diagnosis.

The overall process is visually depicted in Figure 4, where the block diagram illustrates the following workflow:

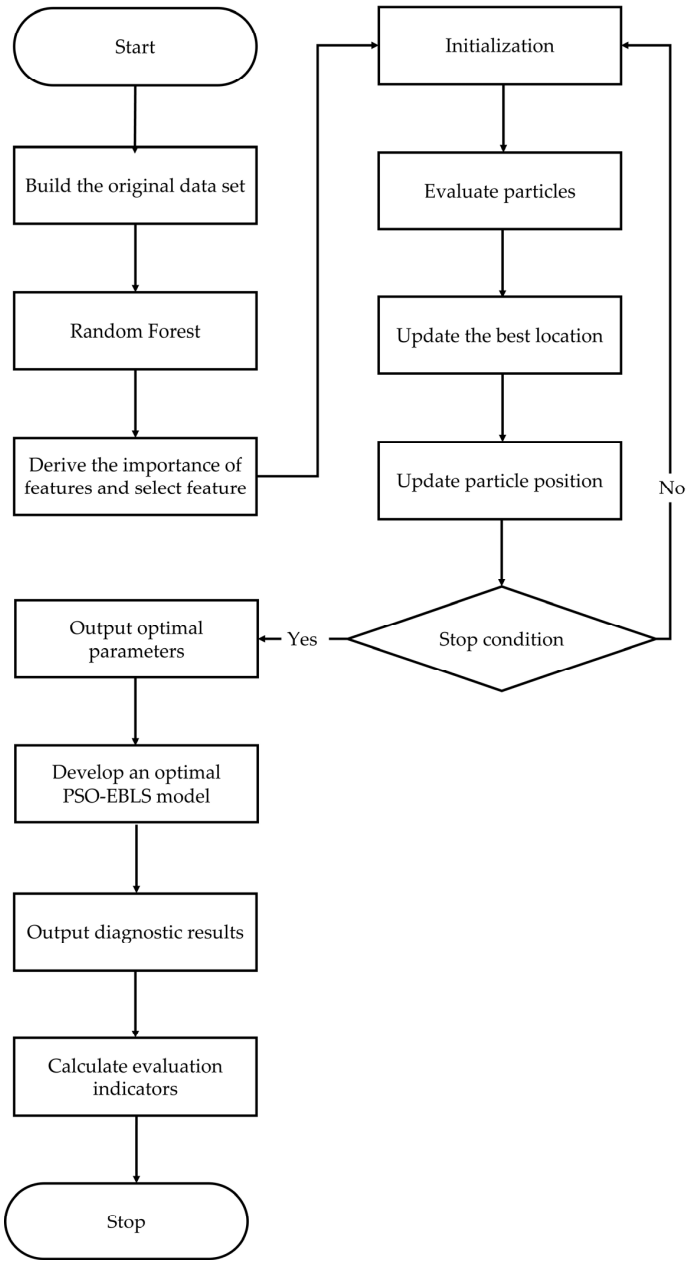

Figure 4. Flowchart of the PSO-EBLS.

(1) Start: The starting point of the process, marking the initialization of the workflow.

(2) Build the original dataset: Construct the original dataset, which includes all relevant data collected from the system to provide the foundation for subsequent processing.

(3) Random Forest: Apply the RF algorithm to process the data, identify the importance of the features, and perform the initial analysis.

(4) Derive the importance of features and select features: Extract the importance of features based on the results from random forest, and select key features for further modeling.

(5) Initialization: Initialize the PSO algorithm by generating the initial particle swarm and their positions.

(6) Evaluate particles: Evaluate the particles by calculating their fitness values in the solution space.

(7) Update the best location: Update the best location within the particle swarm, storing the current optimal solution found so far.

(8) Update particle position: Update the positions of the particles based on the PSO rules for velocity and position updates.

(9) Stop condition: Check if the stop condition is met. If not, return to updating particle positions; if yes, proceed to the next step.

(10) Output optimal parameters: Output the optimal parameters obtained through the PSO optimization for model development.

(11) Develop an optimal PSO-EBLS model: Develop an optimal model based on the PSO-optimized parameters using the EBLS.

(12) Output diagnostic results: Generate diagnostic results, including fault classification of the input data.

(13) Calculate evaluation indicators: Calculate the evaluation metrics to assess the model's performance.

(14) Stop: The endpoint of the process, marking the completion of the entire workflow.

4. Experimental Results and Analysis

In this section, we applied the proposed model in an experimental study aimed at validating its effectiveness. In order to ensure a reliable evaluation of the performance of the proposed model, we conducted the following statistical verification of the results:

4.1. Experiment Data and Environment

4.1.1. Experiment Data

Nuclear power plants are classic examples of SCESs. In this study, we selected the nuclear reactor coolant system (NRCS) of the AP1000, a Generation III+ NPP designed by Westinghouse, as the research object. The NRCS primarily consists of the pressure vessel, pressurizer, steam generator, hot legs, cold legs, and reactor coolant pump. Heat generated in the reactor core is transferred to water in the secondary loop via the steam generator. The cooled reactor coolant is then pumped back into the pressure vessel to complete the cycle. Due to the unique characteristics of NPPs, operational data under accident conditions are extremely scarce. To address this issue, data generated by the personal computer transient analyzer (PCTRAN), as shown in Figure 5, a personal computer-based nuclear power plant simulator, are utilized to validate the accident diagnosis method.

The diagnostic process simulates one normal operating condition (NO) and four typical accident conditions, including a small-break loss of coolant accident (SBLOCA), a large-break loss of coolant accident (LBLOCA), a steam generator tube rupture accident (SGTR), and a loss of flow accident (LOFA), as shown in Table 1. Below is a detailed description of the nature of the samples and the methodology used for their collection:

(1) Nature of the Samples:

(a) NO (L_1): Represents operational data under normal conditions, including steady-state parameters such as coolant temperature, pressure, and flow rate.

(b) SBLOCA (L_2): Represents operational data under partial pipe ruptures with equivalent diameters ranging from 9.5 mm to 25.0 mm. Such accidents result in a gradual coolant leakage, leading to a decrease in both the NRCS pressure and the water level in the pressurizer over time. This gradual loss can also cause an increase in containment temperature and pressure due to heat release at the rupture site.

(c) LBLOCA (L_3): Represents operational data under severe pipe ruptures with equivalent diameters greater than 34.5 mm. This type of accident leads to rapid coolant loss, resulting in abrupt changes in system pressure and temperature.

(d) SGTR (L_4): Represents operational data related to the failure caused by the rupture of one or more U-tubes in the steam generator. Following a SGTR, coolant from the primary loop leaks into the secondary loop, leading to a gradual increase in the radioactive level within the secondary loop. Concurrently, the pressure in the primary loop and the pressurizer water level decrease, while the pressure in the secondary loop rises.

(e) LOFA (L_5): Represents operational data during a coolant flow loss event caused by a main pump failure or shutdown. This results in a decrease in coolant flow, an increase in reactor coolant temperature and pressure, and a rise in pressurizer level.

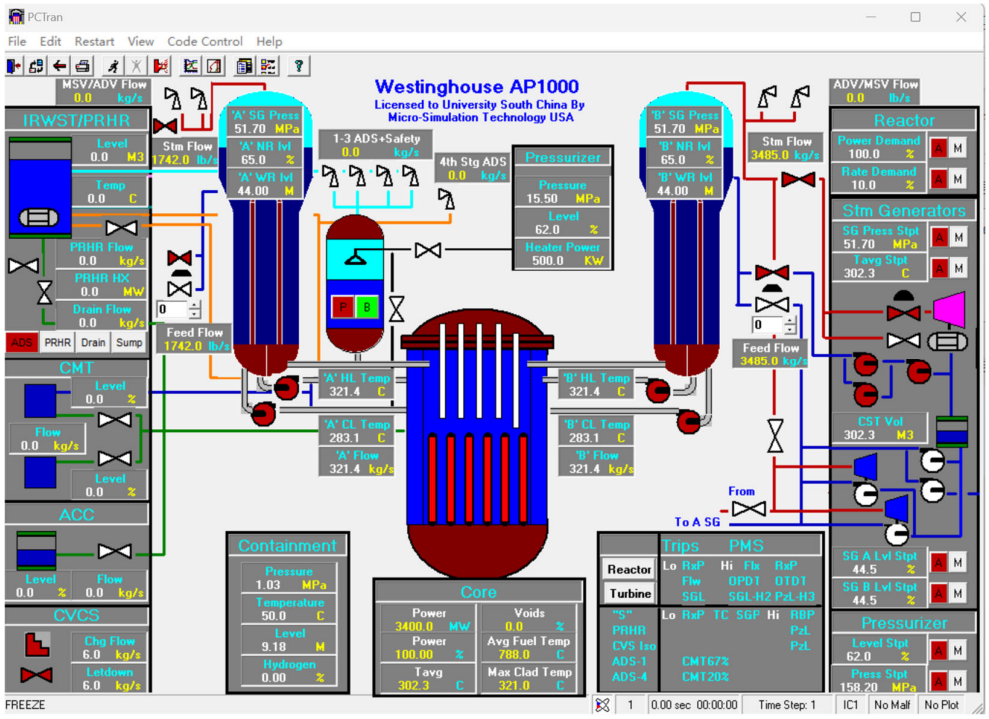

Figure 5. Personal computer transient analyzer.

(2) Sample Collection Methodology:

The samples were generated using PCTRAN, and the steps are as follows:

(a) Simulated Operational Environment: The simulator was configured with operational parameters that mirror real-world NRCS, including a total of 85 fault characteristics.

(b) Data Acquisition: Time series data were collected at regular intervals under different operational and accident scenarios.

(c) Fault Labeling: Based on predefined fault scenarios, the data were labeled into specific categories (L_1–L_5).

To ensure representativeness, multiple simulation runs were performed under varying conditions, creating a high-dimensional, small-sample dataset encompassing both normal and fault states. In our experiment, the PCTRAN simulation reached the normal operational condition within 100 s; after which, it transitioned into four distinct accident scenarios, each running for an additional 100 s. Data were collected at a rate of one sample per second, yielding one hundred samples for each operating condition. Each sample was characterized by 85 features, providing a detailed representation of the system's state at each time step.

Table 1. Description of the fault types.

No.	Fault Type	Name	Labels	Sample Size	Feature Dimension
1	Normal operating	No	L_1	100	85
2	Small-break loss of coolant accident	SBLOCA	L_2	100	85
3	Large-break loss of coolant accident	LBLOCA	L_3	100	85
4	Steam generator tube rupture accident	SGTR	L_4	100	85
5	Loss of flow accident	LOFA	L_5	100	85

4.1.2. Experiment Environment

The conditions required for simulation testing, including the environment and hardware and software configurations, are shown in Table 2.

Table 2. Conditions of the simulation test.

No.	Name	Parameter
1	Emulation device	Lenovo Legion R9000P (2023 Edition) (Lenovo, Hong Kong, China)
2	Central processing unit (CPU)	AMD Ryzen 9 7945HX (AMD, Santa Clara, CA, USA)
3	Graphics processing unit (GPU)	NVIDIA GeForce RTX4060 (NVIDIA, Santa Clara, CA, USA)
4	Operating system	Microsoft Windows 11
5	Simulation software	MATLAB R2023b

4.2. Comparison and Analysis of the Diagnostic Results

4.2.1. Evaluation Metrics

Evaluation metrics are commonly used to assess the performance of diagnostic models. For each category of operating condition, the accuracy, precision, and recall rate are calculated, as shown in Equation (23):

$$\begin{cases} A_i = \frac{(TP_i+TN_i)}{TP_i+FP_i+FN_i+TN_i} \times 100\% \\ P_i = \frac{TP_i}{(TP_i+FP_i)} \times 100\% \\ R_i = \frac{TP_i}{(TP_i+TN_i)} \times 100\% \end{cases} \tag{23}$$

where i denotes the $i-$th operating condition; A_i, P_i, and R_i represent the accuracy, precision, and recall rate of the $i-$th operating condition, respectively; TP_i, FP_i, FN_i, and TN_i correspond to the number of samples diagnosed as the $i-$th operating condition and actually belonging to it, diagnosed as the $i-$th operating condition but actually belonging to other conditions, diagnosed as other conditions but actually belonging to the $i-$th operating condition, and diagnosed as other conditions and actually belonging to other conditions, respectively.

The calculation of accuracy, precision, and recall for all types of operating conditions is given by Equation (24).

$$\begin{cases} \overline{A} = \frac{1}{n}\sum_{i=1}^{n} A_i \\ \overline{P} = \frac{1}{n}\sum_{i=1}^{n} P_i \\ \overline{R} = \frac{1}{n}\sum_{i=1}^{n} R_i \end{cases} \tag{24}$$

where n is the total number of categories of operating conditions categories; $\overline{A}$, $\overline{P}$, and $\overline{R}$ are accuracy, precision, and recall rate, respectively.

4.2.2. Diagnostic Results

To more effectively evaluate the performance of the PSO-EBLS model, five-fold cross-validation was conducted. After completing all five cycles, the average of the verification results was calculated as the final performance metric for the model. The proposed approach was then compared with traditional models, including a convolutional neural network (CNN), support vector machine (SVM), BLS, and EBLS. Table 3 presents a comprehensive list of the key parameters utilized in each method. The results are summarized in Tables 4–7.

The accuracy results from the five-fold cross-validation are presented in Table 4. Significant differences in performance were observed across the models. PSO-EBLS achieved the highest average accuracy at 98.26%, demonstrating its effectiveness in optimizing high-dimensional, small-sample data. This was followed by EBLS, which achieved an average accuracy of 97.40%, benefiting from the ensemble width learning strategy that enhanced both accuracy and stability. In contrast, BLS, SVM, and CNN showed lower average accuracy, with SVM performing particularly poorly on small-sample datasets, which led to a notable decline in performance, reaching only 86.40%.

The precision results from the five-fold cross-validation are presented in Table 5. Both PSO-EBLS and EBLS demonstrated outstanding performance, achieving an average precision of 98.20% and 97.30%, respectively. These models were particularly effective in minimizing false positives during fault diagnosis tasks. Although BLS also achieved high average precision, its performance instability across folds indicated that misclassifications might occur in certain fault scenarios. In contrast, SVM showed lower average precision when dealing with high-dimensional, small-sample data.

The recall rate results from the five-fold cross-validation are presented in Table 6. In terms of recall, PSO-EBLS and EBLS demonstrated superior performance, achieving average recall rates of 98.10% and 97.00%, respectively. These consistently high recall rates ensured comprehensive fault diagnosis, which is crucial for SCESs. While BLS also performed well, its fluctuating recall rate indicated a higher risk of missing faults in certain instances. The lower recall rates observed with SVM and CNN suggest that critical faults may be overlooked.

Table 3. Parameter settings of CNN, SVM, BLS, EBLS, and PSO-EBLS.

Algorithm	Parameter Setting	Value
CNN	Learning Rate	0.001
	Batch Size	32
	Number of Filters	16
	Kernel Size	3×3
	Pooling Size	2×2
	Pooling Stride	2
	Activation Function	ReLU
	Dropout Rate	0.2
	Epochs	100
SVM	Regularization parameter	0.01
	Type of kernel function	Linear
	Kernel parameter	0.001
	Tolerance for optimization	0.0001
BLS	Number of feature node windows	5
	Number of nodes in each feature node window	10
	Number of enhancement nodes	50
EBLS	Number of trees	100
	Maximum depth of each tree	10
	Minimum samples required to be at a leaf node	8
	Minimum samples required to split an internal node	2
PSO-EBLS	Iterations	100
	Population	8
	Inertia weights	0.7
	Individual Learning Factor	2
	Social Learning Factor	2
	Lower band	[10 10 10]
	Upper band	[100 100 100]

Table 4. The accuracies of 5-fold cross-validation.

Model	NO.					
	1 (%)	**2 (%)**	**3 (%)**	**4 (%)**	**5 (%)**	**Average Accuracy (%)**
CNN	92.7	93.2	93.0	93.4	93.1	93.08
SVM	78.00	88.00	90.00	86.00	90.00	86.40
BLS	94.5	97.6	93.8	96.3	95.0	95.44
EBLS	97.2	97.5	97.3	97.6	97.4	97.40
PSO-EBLS	**98.1**	**98.3**	**98.2**	**98.4**	**98.3**	**98.26**

Table 5. The precisions of 5-fold cross-validation.

Model	NO.					
	1 (%)	**2 (%)**	**3 (%)**	**4 (%)**	**5 (%)**	**Average Precision (%)**
CNN	92.8	93.3	92.9	93.4	93.1	93.10
SVM	80.38	89.53	90.10	88.68	90.69	87.88
BLS	94.2	97.8	95.7	96.1	93.9	95.54
EBLS	97.1	97.4	97.2	97.5	97.3	97.30
PSO-EBLS	**98.0**	**98.3**	**98.2**	**98.4**	**98.1**	**98.20**

Table 6. The recall rates of 5-fold cross-validation.

Model	NO.					
	1 (%)	**2 (%)**	**3 (%)**	**4 (%)**	**5 (%)**	**Average Recall Rate (%)**
CNN	92.7	93.2	93.0	93.4	93.1	93.08
SVM	78.00	88.00	90.00	86.00	90.00	86.40
BLS	93.0	97.1	92.5	96.0	94.2	94.56
EBLS	96.8	97.0	96.9	97.2	97.0	97.00
PSO-EBLS	**97.9**	**98.2**	**98.1**	**98.3**	**98.0**	**98.10**

Table 7. The evaluation times of 5-fold cross-validation.

Model	NO.					
	1 (s)	**2 (s)**	**3 (s)**	**4 (s)**	**5 (s)**	**Average Evaluation Time (s)**
CNN	30.5	32.0	31.0	30.7	31.8	31.2
SVM	3.37	3.69	4.02	3.84	3.74	3.73
BLS	**3.4**	**3.3**	**3.5**	**3.3**	**3.4**	**3.38**
EBLS	3.8	3.9	3.7	3.8	3.9	3.82
PSO-EBLS	4.1	4.0	4.2	4.1	4.0	4.08

The evaluation time results from the five-fold cross-validation are presented in Table 7. Regarding time performance, BLS emerged as the fastest model, with an average evaluation time of 3.38 s, making it well suited for real-time applications. EBLS and PSO-EBLS also demonstrated strong efficiency, with average evaluation times of 3.82 s and 4.08 s, respectively, offering a good balance between accuracy and speed. In contrast, SVM and CNN exhibited longer evaluation times, with CNN taking 31.2 s, which limits its suitability for real-time diagnosis.

4.2.3. Comparison and Analysis

Compared to existing methods, the proposed PSO-EBLS model significantly improves fault diagnosis for safety-critical energy systems. Specifically, it achieves an average accuracy of 98.26%, surpassing CNN and SVM by 5.57% and 13.73%, respectively. The evaluation time of PSO-EBLS is 4.08 s—slightly longer than EBLS but much faster than CNN—making it suitable for real-time fault diagnosis.

The superior performance of PSO-EBLS can be attributed to several factors. First, the PSO algorithm efficiently optimizes the EBLS hyperparameters, ensuring stable and accurate predictions. Second, the ensemble strategy in EBLS improves the model robustness by combining multiple random forest-based sub-models. As a result, PSO-EBLS strikes a balance between computational efficiency and diagnostic accuracy, even in high-dimensional, small-sample scenarios.

In contrast, existing approaches such as CNN require extensive training data but suffer from overfitting in small-sample scenarios, resulting in reduced performance. Traditional SVM methods, although robust to small-sample data, have high computational costs and limited scalability. PSO-EBLS, however, excels in handling high-dimensional, small-sample datasets due to its efficient feature extraction and optimization strategies.

In conclusion, PSO-EBLS is the most comprehensive model, excelling in both accuracy and evaluation time, making it the best choice for fault diagnosis in safety-critical energy systems. While EBLS offers excellent accuracy, recall, precision, and evaluation time, it lacks automatic hyperparameter optimization, requiring manual tuning, which reduces efficiency and introduces the potential for suboptimal parameter selection. BLS is well suited for rapid diagnostics with high accuracy but may face performance fluctuations due to stability issues, particularly in high-dimensional, small-sample data. CNN performs well with large datasets but underperforms in small-sample, high-dimensional scenarios. SVM is suitable for small sample data, but its performance is poor in high-dimensional, small-sample data diagnosis, primarily due to its sensitivity to high-dimensional features.

5. Conclusions

This study proposed a novel PSO-EBLS model for IFD in SCESs, particularly focusing on addressing the challenges posed by high-dimensional, small-sample data. By integrating the PSO algorithm with the EBLS, the model achieved significant improvements in accuracy, precision, recall, and computational efficiency compared to traditional methods such as CNN, SVM, and BLS. These advancements demonstrate the potential of PSO-EBLS to enhance fault diagnosis capabilities in SCESs, ensuring higher reliability and operational safety.

The key contributions of this research are summarized as follows:

The study introduced an innovative PSO-EBLS framework that combines RF-based feature selection and ensemble strategies within the BLS architecture, enabling effective modeling for high-dimensional small samples.

By leveraging the PSO algorithm for hyperparameter tuning, the proposed model achieved superior diagnostic accuracy and stability while maintaining computational efficiency.

The model was validated using simulated nuclear power plant (NPP) data, demonstrating its applicability in diagnosing various operating conditions, including normal operation and critical fault scenarios such as SBLOCA and LBLOCA.

However, this study also has certain limitations. Firstly, the experimental data used were generated by a nuclear power plant simulator, and the model's performance in real industrial environments has not yet been verified. Secondly, the inherent data imbalance in SCESs, where normal operating conditions dominate, poses challenges for model generalization. Lastly, while the model demonstrated high efficiency, further optimization is required to ensure scalability for large-scale, high-dimensional datasets.

In the future, several promising directions can be explored:

(1) Developing data augmentation techniques or integrating generative adversarial networks (GANs) to address data imbalance in SCES fault diagnosis.

(2) Exploring hybrid approaches that integrate deep learning-based feature extraction with EBLS to improve performance in multi-modal data scenarios.

In conclusion, the proposed PSO-EBLS model presents a significant step forward in the field of intelligent fault diagnosis for SCESs, offering a robust, efficient, and accurate diagnostic framework. Future research addressing its limitations and expanding its scope will further enhance its potential for practical deployment in diverse industrial environments.

Author Contributions: Methodology, J.Y.; Software, T.D.; Validation, J.Y.; Writing—original draft, J.Y.; Writing—review & editing, J.Y., Y.S. and T.D.; Project administration, Y.S.; Funding acquisition, Y.S. All authors have read and agreed to the published version of the manuscript.

Funding: This research was funded by the National Natural Science Foundation of China, grant number 52174189, and the Natural Science Foundation of Hunan Province, China (2023JJ10035).

Data Availability Statement: The data presented in this study are available on request from the corresponding author.

Acknowledgments: The authors would like to thank PCTRAN for providing the data.

Conflicts of Interest: The authors declare no conflicts of interest.

References

1. Süle, Z.; Baumgartner, J.; Dörgő, G.; Abonyi, J. P-graph-based multi-objective risk analysis and redundancy allocation in safety-critical energy systems. *J. Energy* **2019**, *179*, 989–1003. [CrossRef]
2. Yao, Y.; Han, T.; Yu, J.; Xie, M. Uncertainty-aware deep learning for reliable health monitoring in safety-critical energy systems. *J. Energy* **2024**, *291*, 130419. [CrossRef]
3. Meng, L.; Asuka, J. Impacts of energy transition on life cycle carbon emission and water consumption in Japan's electric sector. *J. Sustain.* **2022**, *14*, 5413. [CrossRef]
4. Gao, Z.; Cecati, C.; Ding, S.X. A survey of fault diagnosis and fault-tolerant techniques—Part I: Fault diagnosis with model-based and signal-based approaches. *J. IEEE Trans. Ind. Electron.* **2015**, *62*, 3757–3767. [CrossRef]
5. Li, J.; Lin, M. Research on robustness of five typical data-driven fault diagnosis models for nuclear power plants. *J. Ann. Nucl. Energy* **2022**, *165*, 108639. [CrossRef]
6. Guo, H.; Hu, S.; Wang, F.; Zhang, L. A novel method for quantitative fault diagnosis of photovoltaic systems based on data-driven. *J. Electr. Power Syst. Res.* **2022**, *210*, 108121. [CrossRef]
7. Lei, Y.; Yang, B.; Jiang, X.; Jia, F.; Li, N.; Nandi, A.K. Applications of machine learning to machine fault diagnosis: A review and roadmap. *J. Mech. Syst. Signal Process.* **2020**, *138*, 106587. [CrossRef]
8. Chen, Z.; Chen, J.; Liu, S.; Feng, Y.; He, S.; Xu, E. Multi-channel Calibrated Transformer with Shifted Windows for few-shot fault diagnosis under sharp speed variation. *J. ISA Trans.* **2022**, *131*, 501–515. [CrossRef] [PubMed]
9. Zhang, T.; Chen, J.; Li, F.; Zhang, K.; Lv, H.; He, S.; Xu, E. Intelligent fault diagnosis of machines with small & imbalanced data: A state-of-the-art review and possible extensions. *J. ISA Trans.* **2022**, *119*, 152–171. [CrossRef]
10. Khentout, N.; Magrotti, G. Fault supervision of nuclear research reactor systems using artificial neural networks: A review with results. *J. Ann. Nucl. Energy* **2023**, *185*, 109684. [CrossRef]
11. Atoui, M.A.; Cohen, A. Coupling data-driven and model-based methods to improve fault diagnosis. *J. Comput. Ind.* **2021**, *128*, 103401. [CrossRef]
12. Irani, F.N.; Soleimani, M.; Yadegar, M.; Meskin, N. Deep transfer learning strategy in intelligent fault diagnosis of gas turbines based on the Koopman operator. *J. Appl. Energy* **2024**, *365*, 123256. [CrossRef]
13. Jiang, F.; Chen, J.; Rong, J.; Liu, W.; Li, H.; Peng, H. Safe reinforcement learning based optimal low-carbon scheduling strategy for multi-energy system. *J. Sustain. Energy Grids Netw.* **2024**, *39*, 101454. [CrossRef]
14. Fang, W.; Zhou, B.; Zhang, Y.; Yu, X.; Jiang, S.; Wei, J. A Fault Diagnosis and Fault-Tolerant Control Method for Current Sensors in Doubly Salient Electromagnetic Motor Drive Systems. *J. IEEE J. Emerg. Sel. Top. Power Electron.* **2024**, *12*, 2234–2248. [CrossRef]
15. Zhang, J.; Zhang, K.; An, Y.; Luo, H.; Yin, S. An integrated multitasking intelligent bearing fault diagnosis scheme based on representation learning under imbalanced sample condition. *J. IEEE Trans. Neural Netw. Learn. Syst.* **2023**, *35*, 6231–6242. [CrossRef]
16. Zheng, Y.; Wang, D. An Auxiliary Classifier Generative Adversarial Network based Fault Diagnosis for Analog Circuit. *J. IEEE Access* **2023**, *11*, 86824–86833. [CrossRef]
17. Jieyang, P.; Kimmig, A.; Dongkun, W.; Niu, Z.; Zhi, F.; Jiahai, W.; Liu, X.; Ovtcharova, J. A systematic review of data-driven approaches to fault diagnosis and early warning. *J. J. Intell. Manuf.* **2023**, *34*, 3277–3304. [CrossRef]

18. Abid, A.; Khan, M.T.; Iqbal, J. A review on fault detection and diagnosis techniques: Basics and beyond. *J. Artif. Intell. Rev.* **2021**, *54*, 3639–3664. [CrossRef]
19. Li, G.; Chen, L.; Fan, C.; Li, T.; Xu, C.; Fang, X. Interpretation and explanation of convolutional neural network-based fault diagnosis model at the feature-level for building energy systems. *J. Energy Build.* **2023**, *295*, 113326. [CrossRef]
20. Zhu, S.; Xia, H.; Annor-Nyarko, M.; Yin, W.; Peng, B.; Wang, Z.; Zhang, J. A robust strategy for sensor fault detection in nuclear power plants based on principal component analysis. *J. Ann. Nucl. Energy* **2021**, *164*, 108621. [CrossRef]
21. Zhang, C.; Tian, X.; Zhao, Y.; Li, T.; Zhou, Y.; Zhang, X. Causal discovery-based external attention in neural networks for accurate and reliable fault detection and diagnosis of building energy systems. *J. Build. Environ.* **2022**, *222*, 109357. [CrossRef]
22. Amiri, A.F.; Oudira, H.; Chouder, A.; Kichou, S. Faults detection and diagnosis of PV systems based on machine learning approach using random forest classifier. *J. Energy Convers. Manag.* **2024**, *301*, 118076. [CrossRef]
23. Et-taleby, A.; Chaibi, Y.; Boussetta, M.; Allouhi, A.; Benslimane, M. A novel fault detection technique for PV systems based on the K-means algorithm, coded wireless Orthogonal Frequency Division Multiplexing and thermal image processing techniques. *J. Sol. Energy* **2022**, *237*, 365–376. [CrossRef]
24. Tuerxun, W.; Chang, X.; Hongyu, G.; Zhijie, J.; Huajian, Z. Fault diagnosis of wind turbines based on a support vector machine optimized by the sparrow search algorithm. *J. IEEE Access* **2021**, *9*, 69307–69315. [CrossRef]
25. Mansouri, M.; Fezai, R.; Trabelsi, M.; Hajji, M.; Harkat, M.F.; Nounou, H.; Nounou, M.; Bouzrara, K. A novel fault diagnosis of uncertain systems based on interval gaussian process regression: Application to wind energy conversion systems. *J. IEEE Access* **2020**, *8*, 219672–219679. [CrossRef]
26. De Santis, E.; Rizzi, A. Modeling failures in smart grids by a bilinear logistic regression approach. *J. Neural Netw.* **2024**, *174*, 106245. [CrossRef]
27. Qiu, S.; Cui, X.; Ping, Z.; Shan, N.; Li, Z.; Bao, X.; Xu, X. Deep learning techniques in intelligent fault diagnosis and prognosis for industrial systems: A review. *J. Sens.* **2023**, *23*, 1305. [CrossRef] [PubMed]
28. Du, Z.; Chen, S.; Li, P.; Chen, K.; Liang, X.; Zhu, X.; Jin, X. Knowledge-extracted deep learning diagnosis and its cloud-based management for multiple faults of chiller. *J. Build. Environ.* **2023**, *235*, 110228. [CrossRef]
29. Seghiour, A.; Abbas, H.A.; Chouder, A.; Rabhi, A. Deep learning method based on autoencoder neural network applied to faults detection and diagnosis of photovoltaic system. *J. Simul. Model. Pract. Theory* **2023**, *123*, 102704. [CrossRef]
30. Harrou, F.; Dairi, A.; Taghezouit, B.; Khaldi, B.; Sun, Y. Automatic fault detection in grid-connected photovoltaic systems via variational autoencoder-based monitoring. *J. Energy Convers. Manag.* **2024**, *314*, 118665. [CrossRef]
31. Gong, X.; Zhang, T.; Chen, C.P.; Liu, Z. Research review for broad learning system: Algorithms, theory, and applications. *J. IEEE Trans. Cybern.* **2021**, *52*, 8922–8950. [CrossRef]
32. Wang, X.; Wang, C.; Zhu, K.; Zhao, X. A Mechanical Equipment Fault Diagnosis Model Based on TSK Fuzzy Broad Learning System. *J. Symmetry* **2022**, *15*, 83. [CrossRef]
33. Chen, C.P.; Liu, Z.; Feng, S. Universal approximation capability of broad learning system and its structural variations. *J. IEEE Trans. Neural Netw. Learn. Syst.* **2018**, *30*, 1191–1204. [CrossRef] [PubMed]
34. Yang, K.; Yu, Z.; Chen, C.P.; Cao, W.; You, J.; Wong, H.S. Incremental weighted ensemble broad learning system for imbalanced data. *J. IEEE Trans. Knowl. Data Eng.* **2021**, *34*, 5809–5824. [CrossRef]
35. Li, K.; Wang, F.; Yang, L.; Liu, R. Deep feature screening: Feature selection for ultra high-dimensional data via deep neural networks. *J. Neurocomputing* **2023**, *538*, 126186. [CrossRef]
36. Pei, W.; Xue, B.; Shang, L.; Zhang, M. Developing interval-based cost-sensitive classifiers by genetic programming for binary high-dimensional unbalanced classification [research frontier]. *J. IEEE Comput. Intell. Mag.* **2021**, *16*, 84–98. [CrossRef]
37. Li, J.; Lin, M.; Li, Y.; Wang, X. Transfer learning network for nuclear power plant fault diagnosis with unlabeled data under varying operating conditions. *J. Energy* **2022**, *254*, 124358. [CrossRef]
38. Li, G.; Yu, Z.; Yang, K.; Chen, C.P.; Li, X. Ensemble-Enhanced Semi-Supervised Learning with Optimized Graph Construction for High-Dimensional Data. *J. IEEE Trans. Pattern Anal. Mach. Intell.* **2024**, *47*, 1103–1119. [CrossRef] [PubMed]
39. Zhao, M.; Ye, N. High-Dimensional Ensemble Learning Classification: An Ensemble Learning Classification Algorithm Based on High-Dimensional Feature Space Reconstruction. *J. Appl. Sci.* **2024**, *14*, 1956. [CrossRef]
40. Zhao, B.; Yang, D.; Karimi, H.R.; Zhou, B.; Feng, S.; Li, G. Filter-wrapper combined feature selection and adaboost-weighted broad learning system for transformer fault diagnosis under imbalanced samples. *J. Neurocomputing* **2023**, *560*, 126803. [CrossRef]
41. Cheng, C.; Wang, W.; Chen, H.; Zhang, B.; Shao, J.; Teng, W. Enhanced fault diagnosis using broad learning for traction systems in high-speed trains. *J. IEEE Trans. Power Electron.* **2020**, *36*, 7461–7469. [CrossRef]
42. Xia, H.; Tang, J.; Yu, W.; Qiao, J. Tree broad learning system for small data modeling. *J. IEEE Trans. Neural Netw. Learn. Syst.* **2022**, *35*, 8909–8923. [CrossRef] [PubMed]
43. Wu, J.; Chen, X.Y.; Zhang, H.; Xiong, L.D.; Lei, H.; Deng, S.H. Hyperparameter optimization for machine learning models based on Bayesian optimization. *J. J. Electron. Sci. Technol.* **2019**, *17*, 26–40. [CrossRef]

44. Viswanathan, S.; Ravichandran, K.S. Gain-based Green Ant Colony Optimization for 3D Path Planning on Remote Sensing Images. *J. Spectr. Oper. Res.* **2025**, *2*, 92–113. [CrossRef]
45. Mzili, T.; Mzili, I.; Riffi, M.E.; Pamucar, D.; Simic, V.; Kurdi, M. A novel discrete rat swarm optimization algorithm for the quadratic assignment problem. *J. Facta Univ. Ser. Mech. Eng.* **2023**, *21*, 529–552. [CrossRef]
46. Mzili, T.; Mzili, I.; Riffi, M.E.; Dragan, P.; Vladimir, S.; Laith, A.; Bandar, A. Hybrid genetic and penguin search optimization algorithm (GA-PSEOA) for efficient flow shop scheduling solutions. *J. Facta Univ. Ser. Mech. Eng.* **2024**, *22*, 77–100. [CrossRef]
47. Zhao, F.; Ji, F.; Xu, T.; Zhu, N. Hierarchical parallel search with automatic parameter configuration for particle swarm optimization. *J. Appl. Soft Comput.* **2024**, *151*, 111126. [CrossRef]